and thus at the rear contact ($x = d$) it is :

$$\frac{d\mathcal{E}}{dt} = \frac{q_o A d}{2\epsilon_S}\frac{dn_T(t)}{dt}. \tag{4.58}$$

Combining eqs. 4.54, 4.55, 4.58 one gets for the thermally stimulated current :

$$I_{TSC} = -\frac{qAd}{2}\frac{dn_T(t)}{dt}. \tag{4.59}$$

The change of n_T per unit time in the SCR is given in eq. 2.54. In the following $e_p \ll e_n$ is assumed and hence

$$I_{TSC} = \frac{qAd}{2}e_n n_T(t). \tag{4.60}$$

In this case the current is proportional to the emission rate for electrons and to the number of occupied traps. If $e_p \gg e_n$ the current is proportional to the emission rate for holes and to the number of non-occupied traps. Because the sign of I_{TSC} is the same in both cases it is not possible to distinguish between electron and hole emission.

The emission rate e_n is already given in eq. 2.42 and the number of occupied traps as function of time is :

$$n_T(t) = n_{T,0}\exp\left(-\int_0^t e_n dt\right), \tag{4.61}$$

with $n_{T,0}$ being the number of occupied traps at $t = 0$. If the temperature is kept constant ($dT/dt = 0$) eq. 4.61 results in eq. 4.15 and the measured current decreases exponentially [8]. But during the TSC-measurement the temperature increases from the initial temperature T_i with a heating rate $\beta(T) = dT/dt$. Substituting t by $T = T_i + \beta(T)t$ in eq. 4.61 one gets

$$n_T(T) = n_{T,0}\exp\left(-\int_{T_i}^T e_n(T')\frac{1}{\beta(T)}dT'\right). \tag{4.62}$$

Using this explicit expression for n_T in eq. 4.60 the thermally stimulated current can be written as function of temperature :

$$I_{TSC}(T) = \frac{qAd}{2}e_n(T)n_{T,0}\exp\left(-\int_{T_i}^T e_n(T')\frac{1}{\beta(T)}dT'\right). \tag{4.63}$$

This function is plotted in fig. 4.12. Additionally the concentration of occupied traps is shown in the same figure. It can be seen that in the beginning the current

[8] I-DLTS

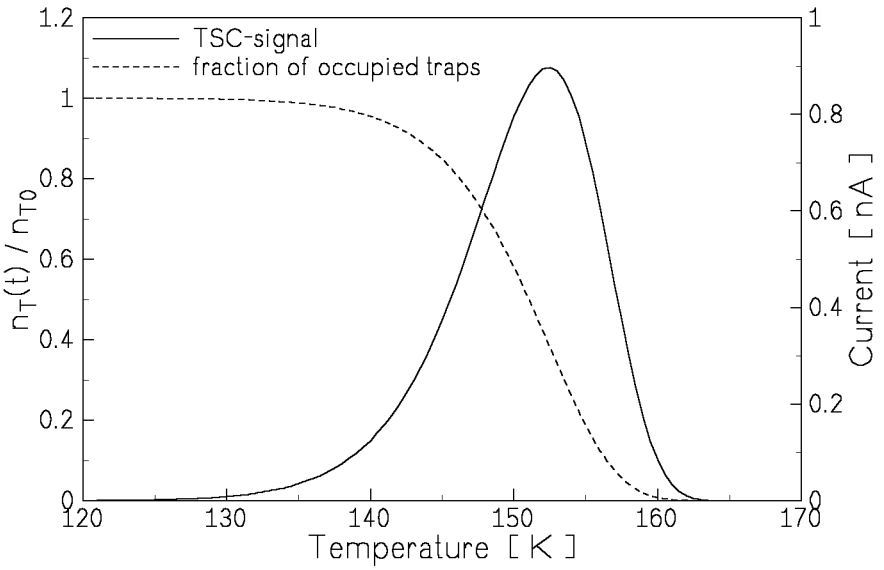

Figure 4.12: TSC-signal (solid line) and number of occupied traps (broken line) as function of temperature.

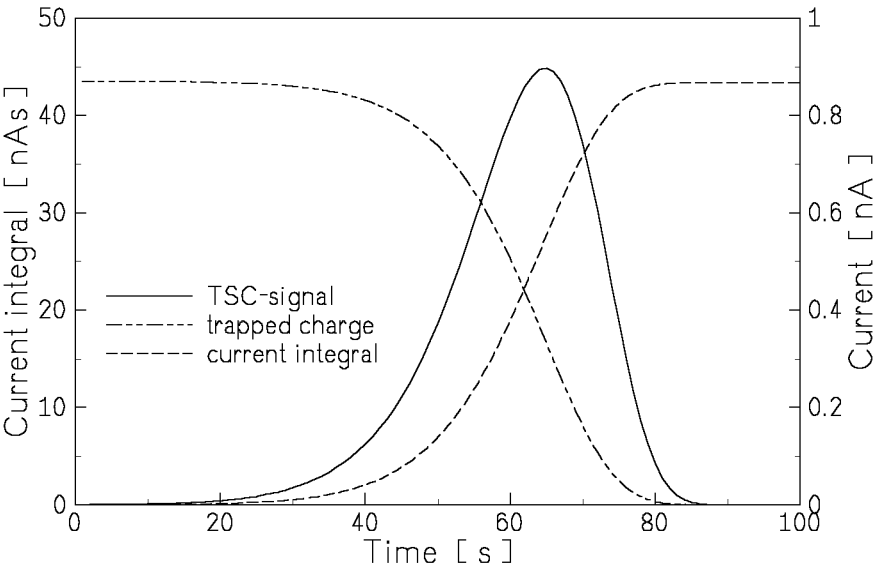

Figure 4.13: TSC-signal (right Y-axis), amount of trapped charge and current integral as function of time (left Y-axis).

increases with temperature due to the increasing emission rate, reaches a maximum at $T = T_m$ and then decreases, because the number of occupied traps becomes smaller.

In fig. 4.13 the TSC-signal is plotted as function of time. In addition, the amount of trapped charge is shown and the current integral $\int_{t_i}^{t} I_{TSC} dt$, which equals the emitted charge at time t. Note, that the final integral over current is equivalent to the total emitted charge and thus proportional to the concentration of occupied traps $n_{T,0}$:

$$Q_{tot} = \int_{t=0}^{t_{end}} I_{TSC} dt = n_{T,0} \frac{qAd}{2}. \tag{4.64}$$

Directly from the integral the number of occupied traps can be deduced :

$$n_{T,0} = \frac{2}{qAd} \int_{t=0}^{t_{end}} I_{TSC} dt = \frac{2Q_{tot}}{qAd}. \tag{4.65}$$

In contrast to DLTS the TSC-method is not restricted to defect concentrations which are small in comparison to the free charge carrier concentration, but a higher number of defects will result in a higher peak. The detection of small concentrations is limited only by the current noise of the sample and the sensitivity of the Ampere meter. A typical value of leakage current at T <140 K is 5 pA cm^{-3} fluctuating in a range of $\pm$2 pA cm^{-3}. In order to obtain a clear peak for the analysis the current in peak maximum should be greater by a factor of ten. Thus for the samples under investigation (d =300 μm and A =0.25 cm^2, see sec. 5.1) and typical heating rates (0.5 to 1.0 Ks^{-1}) the detection limit of TSC can be estimated to be in the range of 10^{10} cm^{-3}.

4.3.2 Determination of Energy Level Parameters

4.3.2.1 Method of Delayed Heating

The method of delayed heating has been introduced by Muller et al. [88] in 1974. The TSC-peak is measured several times from the same initial temperature T_i and for each measurement the delay between the filling and the start of the heating is extended. Because during this delay trapped charges are already emitted at T_i ($e_n \propto \exp(-\Delta E_T / k_B T_i)$) the number of occupied traps $n_{T,0}$ becomes smaller the longer the delay lasts. As can be seen from eq. 4.63 this leads also to a smaller thermally stimulated current. Thus, if the peak height or the peak integral is plotted vs. the time of delay t_d (which is also called de-excitation time) the emission time constant $\tau(T)$ is given directly by the slope (see fig. 4.14). Repeating this procedure of determing τ at different temperatures T_i, ΔE_T can be obtained with the Arrhenius-Ansatz.

The advantage of this method is that the emission rates are measured at a constant temperature. All other methods presented here depend on a very exact measurement of the temperature while it is changing very rapidly.

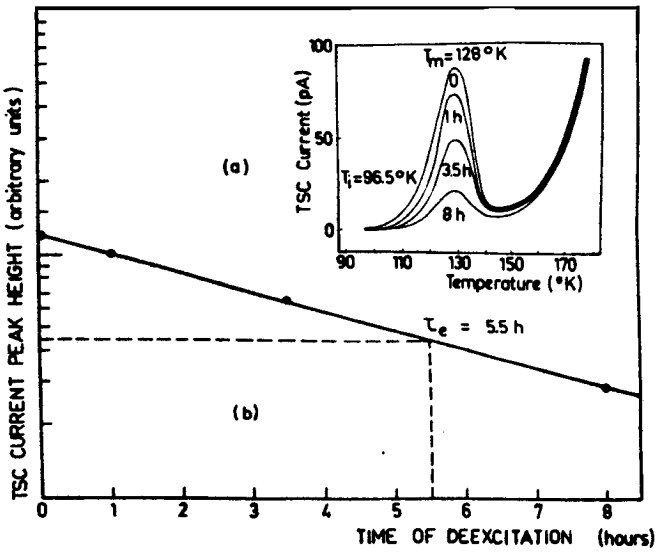

Figure 4.14: Method of delayed heating after Muller [88].

4.3.2.2 The Deconvolution Method

The methods described above are restricted to peaks which are not or only negligible overlapped by other peaks. But, if the TSC spectrum becomes complex it has to be re-calculated to deconvolute the parameters $\Delta E_T, \sigma$ and $n_{T,0}$ of each level supposed to be part of the spectrum [89, 90]. In case of several levels contributing to the thermally stimulated current the measured spectrum is the sum of the currents caused by each level. Let m be the total number of levels and $\Delta E_{T,l}, \sigma_l, n_{T,l}$ parameters of the level l. Then the current at temperature T is :

$$I_{TSC}(T) = \frac{qAd}{2\epsilon_S} \sum_{l=0}^{m} e(T, \Delta E_{T,l}, \sigma_l) n_{T,0,l} \exp\left(- \int_{T_i}^{T} e(T' \Delta E_{T,l}, \sigma_l) \frac{1}{\beta} dT' \right) . \quad (4.66)$$

By choosing a reasonable set of parameters for each level a spectrum can be calculated applying eq. 4.66. If the first approach does not fit the data, the parameters have to be varied until the fit is satisfying. An example is shown in fig. 4.15.

One of the major problems of this method is the number of levels. The minimum number can be obtained by counting the peaks visible in the spectrum. But little can be known about levels which are hidden in the spectrum. However, the choice of reasonable parameters becomes less difficult, if several spectra measured under different conditions (e.g. β, T_i, filling pulse) are compared or results of other methods are used for input.

4.3.2.3 Integral Analysis of a Single Peak

The fourth method of analysis described here requires only one TSC-measurement to determine $\Delta E_T, \sigma, n_T$. The total charge from a certain level is given by eq. 4.64. In fig. 4.16 the area below the peak is divided into two parts. The left side gives the

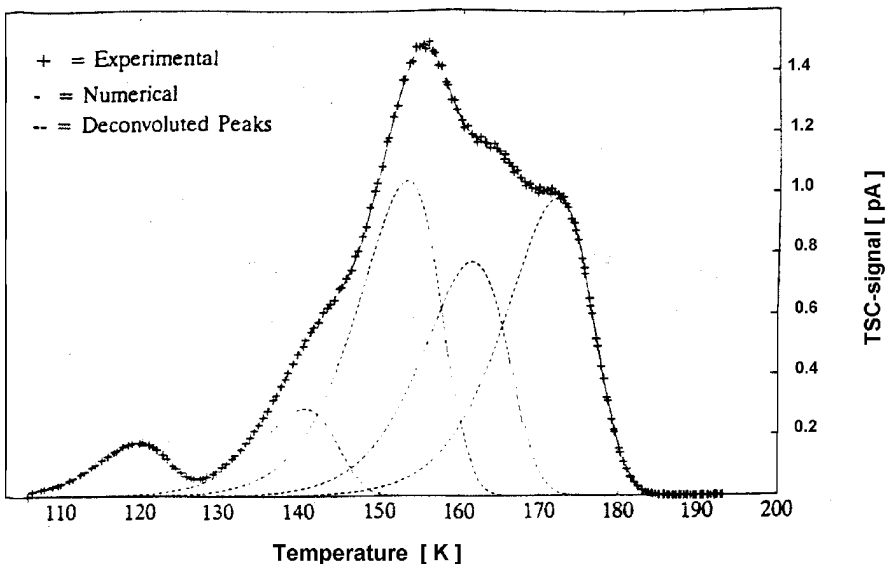

Figure 4.15: The deconvolution method after Biggeri [90].

amount of charge which has already been released at time t_x ($t_0 < t_x < t_{end}$), while the right side gives the charge, which is still trapped in the level at t_x. This charge Q_x is given by :

$$Q_x = \int_{t_x}^{t_{end}} I_{TSC} dt = n_T(t_x) \frac{qAd}{2} \tag{4.67}$$

and one gets :

$$n_T(t_x) = \frac{2}{qAd} \int_{t_x}^{t_{end}} I_{TSC} dt \tag{4.68}$$

The current at time t_x is given by eq. 4.60 :

$$I_{TSC}(t_x) = \frac{qAd}{2} e(t_x) n_T(t_x), \tag{4.69}$$

which can be resolved to

$$e(t_x) = \frac{2 I_{TSC}(t_x)}{qAd n_T(t_x)}. \tag{4.70}$$

If $n_T(t_x)$ on the right hand side is replaced by the expression given in eq. 4.68 it follows :

$$e(t_x) = \frac{I_{TSC}(t_x)}{\int_{t_x}^{t_{end}} I_{TSC} dt}. \tag{4.71}$$

Because t_x corresponds to a temperature T_x, eq. 4.71 implies the dependence of the emission rate on the temperature, and thus ΔE_T and σ can be obtained with the Arrhenius-Ansatz. This is shown in fig. 4.17. $n_{T,0}$ is given by eq. 4.64.

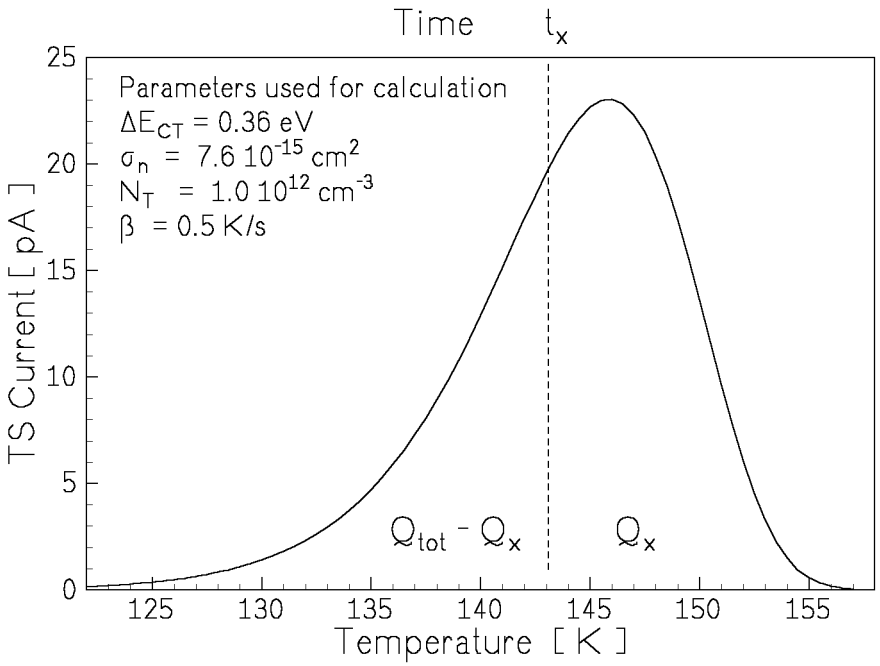

Figure 4.16: TSC-peak divided into two parts at time t_x.

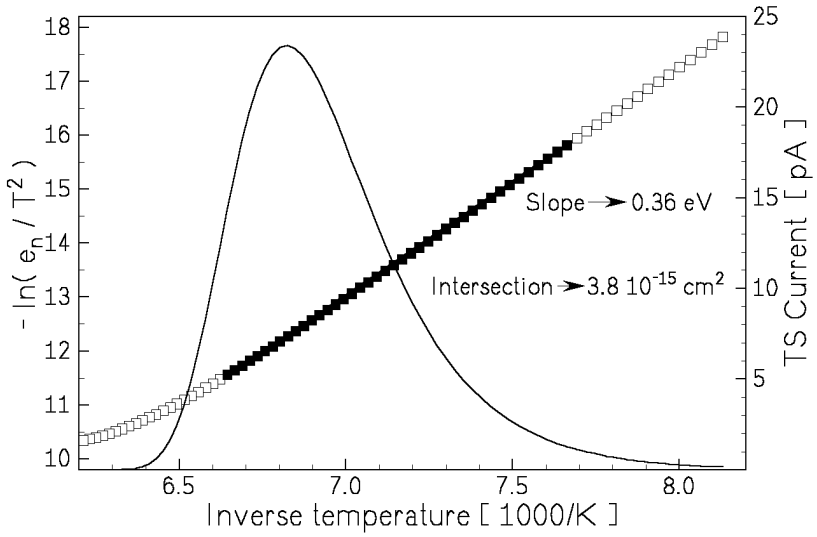

Figure 4.17: TSC-signal (solid line, right Y-axis) and corresponding Arrhenius plot as obtained from the integral analysis (left axis). The filled squares were used for fit.

4.3.2.4 Variation of the Heating Rate

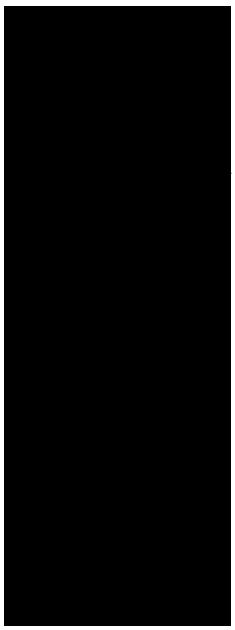

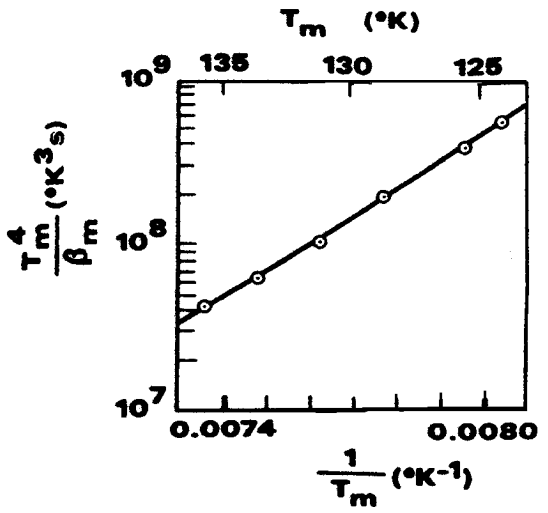

Figure 4.18: Left : TS-current from gold donors in a silicon n^+-p junction for various heating rates. Right : Analysis of the emission rate as described in the text [87].

For completeness the method of variation of the heating rate shall also be described here, although it has not been used. To determine the energy level of a trap Buehler [87] used the variation of the heating rate to shift the maximum of the TSC-peak. The peak maximum is defined by :

$$\frac{dI_{TSC}(t,T_m)}{dt} = 0. \tag{4.72}$$

Then from eq. 4.60 it follows :

$$\frac{d(e_n n_T(t))}{dt} = \frac{e_n}{dt} n_T(t) + e_n \frac{dn_T(t)}{dt} = 0. \tag{4.73}$$

If $e_n \gg e_p$ and hence $-r_b \gg r_d$ one gets with eqs. 2.37 and 2.52:

$$\frac{d(e_n(t))}{dt} = e_n^2(t). \tag{4.74}$$

Replacing $\sigma_n v_{th} N_C$ in eq. 2.42 by $B_n T_m^2(t)$ one gets :

$$\frac{d(e_n(t)}{dt} = B_n \beta T_m \exp\left(-\frac{\Delta E_T}{k_B T_m}\right)(2 - \frac{\Delta E_T}{k_B T_m}) \tag{4.75}$$

Equating this expression to the square of $e_n(t)$ and solving for $\frac{T_m^4}{\beta(T_m)}$ leads to :

$$\frac{T_m^4}{\beta(T_m)} = \exp\left(-\frac{\Delta E_T}{k_B T_m}\right) + \frac{\Delta E_T}{k_B B_n} + (1 - \frac{2k_B T_m}{\Delta E_T}). \tag{4.76}$$

If the last term on the right side is neglected, ΔE can be determined from the slope of a plot $\ln \frac{T_m^4}{\beta(T_m)}$ vs. $\frac{1}{T_m}$. The cross section can be calculated from $B_n(\frac{1}{T_m} = 0)$. An example of the method is shown in fig. 4.18. It should be emphazised that the heating rate does not have to be constant.

4.4 Heat Treatments

Heat treatment or tempering experiments were performed to investigate the long term behaviour of the detector properties, especially of the effective doping concentration. Assuming one or more annealing processes to be responsible for the change of N_{eff} the time scale can be compressed significantly by tempering, since the time dependence is governed by the reaction constant (see sec. 3.2):

$$k(T) = k_0 \exp\left(\frac{-E_a}{k_B T}\right). \tag{4.77}$$

The reverse annealing (see sec. 6.1.2) e.g. at room temperature takes years to reach the final value, while it lasts only days if the temperature is elevated to 80°C. The possibility to compress the time scale is of utmost importance for the ability to forecast the long term detector performance in HEP-experiments.

To gain a more detailed insight into the annealing processes it is necessary to perform isothermal and isochronal heat treatments systematically.

4.4.1 Isothermal Heat Treatments

For an isothermal heat treatment the sample under investigation is kept at a certain temperature T. Only to measure the quantity $\mathcal{Q}$ of interest the sample is cooled to room temperature. Thus one gets $\mathcal{Q}(t, T)$ and the time dependence at temperature T can be fitted. The most simple isothermal heat treatments are those at room temperature. Of course measurements made at lower temperature can also be noted as isothermal. But the measurement of the sample at room temperature should be avoided, because the change of $\mathcal{Q}$ might be enhanced, thus disturbing the determination of the time dependence. In case of a first order process the result will be a time constant τ, or a reaction constant $\hat{k}$ respectively. The dependence of the reaction constant on the temperature can be obtained, if heat treatments at different temperatures are performed. From eq. 4.77 it follows that

$$\ln \hat{k}(T) = \ln \hat{k}_0 + \left(\frac{-E_a}{kT}\right). \tag{4.78}$$

If $\ln \hat{k}(T)$ is plotted versus $1/kT$ the activation energy E_a is given by the slope (Arrhenius-relation).

If the process is of second order the above given procedure can be applied in a corresponding way. Of course in both cases, first or second order, the Arrhenius plot will give no straight line if more than one process with similar reaction behaviour occur. Hence, the temperature range is often limited to those temperatures at which other processes depend only weakly on T.

4.4.2 Isochronal Heat Treatments

Another technique to determine the annealing parameters is the isochronal heat treatment. Instead of the temperature, the duration of each tempering step is kept constant. Let's assume a concentration N can be changed by tempering, then each tempering step i of duration t_i at a temperature T_i can be described by a tripel T_i, t_i, N_i, where the last figure N_i gives the concentration after the ith tempering step. In case of a first order process the change of N can be deduced from eq. 3.6 :

$$N_i = N_{i-1} \exp(-t_i \hat{k}(T_i)). \tag{4.79}$$

The corresponding equation for the second order case is (see eq. 3.12) :

$$N_i = \frac{N_{i-1}}{1 + N_{i-1} t_i \tilde{k}(T_i)}. \tag{4.80}$$

After resolving both equations for $t_i k(T_i)$ the reaction constant has to be replaced by its explicit expression as it is given in eq. 3.4. This leads to :

$$\ln\left(\frac{N_i}{N_{i-1}}\right) = -t_i \hat{k}_0 \exp\left(\frac{-E_a}{k_B T_i}\right) \qquad 1.\ \text{order}, \tag{4.81}$$

and

$$\frac{1}{N_i} - \frac{1}{N_{i-1}} = t_i \tilde{k}_0 \exp\left(\frac{-E_a}{k_B T_i}\right) \qquad 2.\ \text{order}. \tag{4.82}$$

After applying the logarithmus function one gets :

$$\underbrace{\ln\left(\ln\left(\frac{N_i}{N_{i-1}}\right)\right)}_{\gamma_1} = \ln(-t_i \hat{k}_0) - \frac{E_a}{k_B T_i} \qquad 1.\ \text{order}, \tag{4.83}$$

and

$$\underbrace{\ln\left(\frac{1}{N_i} - \frac{1}{N_{i-1}}\right)}_{\gamma_2} = \ln(t_i \tilde{k}_0) - \frac{E_a}{k_B T_i} \qquad 2.\ \text{order}. \tag{4.84}$$

Both terms, γ_1 and γ_2 which are expected to depend linearly on the inverse temperature if either the first or second order assumption applies are very different. Hence a comparison of plots corresponding to eqs. 4.83 and 4.84 may help to decide between the first and second order model.

Chapter 5

Experimental Equipment

5.1 Samples, Detectors, and Devices under Test

The radiation induced change of detector properties has been investigated using surface barrier (SB) and ion implanted p^+-n -detectors. The high resistivity silicon was mainly n-type, a few p-type samples were used to compare some features of inverted n-type material.

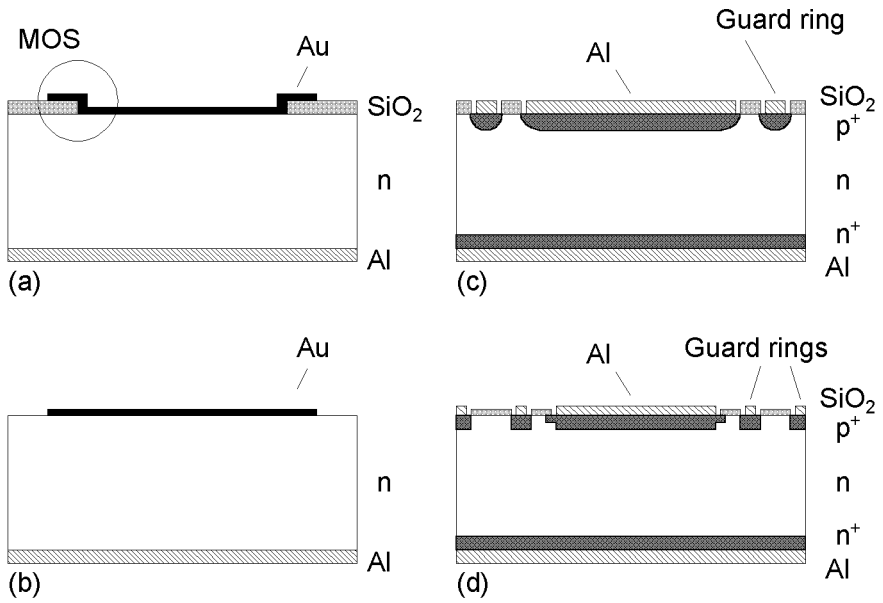

Figure 5.1: The four types of detector test structures shown schematically in section (diagram not true to scale). (a) : Surface barrier detector with oxide and (b) without oxide passivation. For the p-type samples replace n by p. (c) : p^+-n -detector from Micron or Intertechnique, respectively, and (d) from MPI (see text).

The SB-detectors (i.e Schottky diodes) were fabricated in the laboratory of the *Gruppe Nukleare Messtechnik, Hamburg* [91] in cooperation with *Kemtek* [92] and *Forschungszentrum Rossendorf* [93]. The process is described already in [16]. A schematic section of the different structures is shown in fig. 5.1. Note, that the

gold electrode overlaps the oxide. Thus the edge of the electrode behaves like a MOS-structure.

The p^+-n -detectors were supplied by *Micron* [94], *Intertechnique* [95] and the *Max Planck Institut München* [1] (MPI) [96]. Sections of the structure can be seen also in fig. 5.1. The Micron and Intertechnique detectors were made using the same mask, but different passivations.

While the TSC-measurements were also made on such high resistivity material, for DLTS-measurements material of lower resitivity has been used additionally. For special purposes material has also been investigated which was not oxide-passivated (see sec. 7.1.1).

Sample specifications such as geometry and material properties are listed in tab. 5.1. Note, that the starting material is produced by *Wacker* [97] in any case. For easier handling most of the samples were mounted on chip carriers or ceramics

Specification			ρ [Ωcm]	$N_{eff,0}$ [cm^{-3}]	d [μm]	A [cm^2]	Form	Label
SB	n	ox	7000	$6 \cdot 10^{11}$	390	0.44*,0.16*	C	901 etc
SB	n	nox	6	$8 \cdot 10^{14}$	400			933
SB	n	ox	9000	$5 \cdot 10^{11}$	330			935
SB	n	ox	9000	$5 \cdot 10^{11}$	510			934
SB	p	ox	6000	$7 \cdot 10^{11}$	300			936
SB	n	nox	100	$4 \cdot 10^{13}$	230			938
SB	n	nox	4000	$1 \cdot 10^{12}$	400			939
SB	n	nox	2000	$3 \cdot 10^{12}$	390			93A
p^+-n	n	ox	9000	$5 \cdot 10^{11}$	310	0.25	Q	MUE
p^+-n	n	ox	9000	$5 \cdot 10^{11}$	300		Q	INT
p^+-n	n	ox	3000	$2 \cdot 10^{12}$	280		Q,C	M1, M2

Table 5.1: Detectors used for the investigation.
Specifications : n, p : n-type and p-type material respectively, ox : oxide-passivated, nox : no oxide. Q : square (pure geometrical extension), C : circle (geometrical extension plus lateral extension, * labelled G, * labelled K).

with special pins to make plug-in contacts. The samples used for DLTS or TSC were not mounted, but contacted by probe needles (see sec. 5.4).

5.2 Irradiation Facilities

The irradiation experiments were performed at the *Physikalisch-Technische Bundesanstalt* (PTB) in Braunschweig and at the *Universitätskrankenhaus Eppendorf* (UKE) in Hamburg [2].

[1] The MPI-München is member of the ATLAS- collaboration.
[2] University Hospital Hamburg